nature energy

ARTICLES

https://doi.org/10.1038/s41560-017-0068-x

Spatial decoupling of light absorption and catalytic activity of Ni–Mo-loaded high-aspect-ratio silicon microwire photocathodes

Wouter Vijselaar[1], Pieter Westerik[2], Janneke Veerbeek[1], Roald M. Tiggelaar[2,3], Erwin Berenschot[2], Niels R. Tas[2], Han Gardeniers[2]* and Jurriaan Huskens[1]*

A solar-driven photoelectrochemical cell provides a promising approach to enable the large-scale conversion and storage of solar energy, but requires the use of Earth-abundant materials. Earth-abundant catalysts for the hydrogen evolution reaction, for example nickel–molybdenum (Ni–Mo), are generally opaque and require high mass loading to obtain high catalytic activity, which in turn leads to parasitic light absorption for the underlying photoabsorber (for example silicon), thus limiting production of hydrogen. Here, we show the fabrication of a highly efficient photocathode by spatially and functionally decoupling light absorption and catalytic activity. Varying the fraction of catalyst coverage over the microwires, and the pitch between the microwires, makes it possible to deconvolute the contributions of catalytic activity and light absorption to the overall device performance. This approach provided a silicon microwire photocathode that exhibited a near-ideal short-circuit photocurrent density of 35.5 mA cm^{-2}, a photovoltage of 495 mV and a fill factor of 62% under AM 1.5G illumination, resulting in an ideal regenerative cell efficiency of 10.8%.

A good solar-to-fuel device is efficient both in light harvesting and in transforming the photogenerated electricity into chemical bonds. Silicon (Si) is a popular, high-performing photon absorber. However, Si as a photocathode has poor kinetics for the hydrogen evolution reaction (HER)[1] and therefore requires a catalyst to achieve efficient solar-to-hydrogen conversion. Unfortunately, however, for state-of-the-art Earth-abundant catalysts (such as Ni–Mo), the high mass loading that is needed for sufficient catalytic activity also results in considerable parasitic light absorption upon frontside illumination, which reduces the efficiency of such photocathodes.

One promising route to obtain high efficiencies for systems consisting of semiconductors coated with a catalytic material is by spatially and functionally decoupling the optical absorption and the catalytic activity of the photocathode. Silicon microwire arrays provide an approach to overcome the negative correlation between the catalytic activity, which is directly related to the fill factor, FF, in terms of photovoltaic (PV) cells, and light absorption, J_{ph}. High FF values in Si microwire photocathodes have been obtained by covering the bottom area between the microwires with Ni–Mo/TiO_2 (ref. [2]) or cobalt phosphide nanoparticles[2,3]. The best-performing Si homojunction microwire array photocathodes from these studies demonstrated an ideal regenerative cell efficiency, η_{irc}, of 2.9 and 2.8% respectively[2–4]. These efficiencies, obtained in designs without surface passivation, were restricted by light absorption, evidenced by a limited photocurrent (<15 mA cm^{-2}), whereas passivated Si PV cells easily generate about 40 mA cm^{-2} (refs [5,6]). Surface passivation suppresses recombination of charge carriers at the surface. This becomes increasingly important as the absolute surface area increases, which is the case especially for high-aspect-ratio structures.

By studying ultramicroelectrode arrays of platinum (Pt) disks on n^+-Si, it was found that placing catalyst islands as far as 12 µm apart did not significantly increase the kinetic overpotential of the HER, but that, beyond that distance, catalyst performance went down[7]. Although this study was limited to a two-dimensional (2D) surface, it is clear that the spacing of separate catalyst islands can strongly influence the catalyst performance of any photocathode. Because this might also hold for the 3D photocathodes discussed in the present paper, we investigate the influence of microwire pitch (centre-to-centre distance between the microwires) on performance of these devices.

Here we describe the spatial and functional decoupling of light absorption and catalytic activity of frontside-illuminated Si microwire array photocathodes. Radially doped microwire arrays are passivated by SiO_2, which increases the efficiency of the underlying PV cell[6,8,9]. The SiO_2 is spatioselectively removed from the top sides of the microwire arrays. The remaining, insulating SiO_2 layer acts as a masking layer in a subsequent process step in which the freshly exposed Si top is covered with an electrodeposited catalyst for H_2 production. The influence of the size of the catalyst-covered region and the spacing between the microwires on the performance of the resulting photocathodes was investigated, by measuring their photovoltaic (J–V, where J is current density and V voltage), electrochemical and photo-electrochemical (J–E), where E is potential versus RHE) characteristics. Variation and comparison of the different device parameters results in a deeper understanding of the limiting factors in photocathode performance, leading to an optimized design with an ideal regenerative cell efficiency, η_{IRC}, of >10%.

Spatioselective coating of on microwires

Substrates with arrays of silicon microwires (4 µm diameter, 40 µm length and 6 µm pitch) with radial junctions (p-type base and 900 nm

[1]Molecular NanoFabrication, MESA+ Institute for Nanotechnology, University of Twente, Enschede, The Netherlands. [2]Mesoscale Chemical Systems, MESA+ Institute for Nanotechnology, University of Twente, Enschede, The Netherlands. [3]NanoLab Cleanroom, MESA+ Institute for Nanotechnology, University of Twente, Enschede, The Netherlands. *e-mail: j.g.e.gardeniers@utwente.nl; j.huskens@utwente.nl

n$^+$-type emitter) were fabricated according to a procedure reported previously[8]. The microwire length was chosen to provide optimal light absorption[9]. The substrates were processed in one of three ways. To deposit a catalyst over the entire surface of the Si microwire arrays (Fig. 1a), the arrays were subjected to electrodeposition without further preparation. For selective deposition near the tops of the microwires (Fig. 1b), the wires were first conformally covered with SiO_2, followed by a photoresist layer, which was etched back in O_2 plasma to expose the tops of the wires. Subsequently, the exposed SiO_2 layer was etched in buffered hydrogen fluoride (BHF) (see Methods for details). For the electrodeposition of catalyst that covered more of the microwires from the top down, we used selective removal of SiO_2 from the tops of the microwires by inclined ion beam etching, and retraction of sacrificial layers (a combination of polysilicon and silicon nitride) to the desired height *X*, as measured from the top of the microwire (Fig. 1c; see Methods for details).

Homogeneous electrodeposition of bright nickel (Ni) over 3D microstructures, such as Si microwires, has been described before[10]. The addition of a relatively low concentration of Na_2MoO_4 (24 mM) to the $NiSO_4$ (1.3 M) deposition bath, to form Ni–Mo, alters the composition and growth morphology of the layer[11,12]. High-resolution scanning electron microscope (HR-SEM) images reveal that electrodeposition of Ni–Mo in the range of 10 to 180 s does not lead to a continuous thin film on bare Si microwire arrays; instead, isolated particles are deposited all over the surface (Fig. 1d). The difference in growth morphology between the two materials (Ni versus Ni–Mo) is attributed to the low current efficiency, which is below 5% in the case of Ni–Mo deposition, as compared with nearly 100% under the conditions for Ni deposition from a sulfate solution[13–17]. Furthermore, it was observed that the Ni–Mo particles at the tops of the microwires agglomerate slightly, whereas, at the bottom, individual particles are evenly distributed over the surface (Supplementary Fig. 1).

The crystal structure of the deposited Ni–Mo films was confirmed by X-ray diffraction (XRD) (Supplementary Fig. 2)[18]. Films of Ni–Mo were compared with electrodeposited Ni films and a reference pattern, and it was found that both the (111) and (002) peaks of Ni–Mo were shifted relative to the Ni pattern[19]. This is in line with reports that Mo cannot be deposited as a pure metal from an electrodeposition bath and only occurs in co-deposition with another metal such as nickel[15–17]. Previous research[19] indicated that this Ni–Mo alloy has 9% of molybdenum incorporated in the structure: that is, $Ni_{0.91}$–$Mo_{0.09}$.

Figure 1e presents an HR-SEM image of a Si microwire with high mass loading of Ni–Mo solely at the upper ~2 µm, and Fig. 1f shows a zoom-out of the corresponding microwire array. The results confirm that, during the electrodeposition process, the insulating layer of SiO_2 effectively inhibits the transfer of electrons at the wire surface area below the exposed tops, thereby restricting catalyst deposition to the top side of the microwire arrays. Similar to what was observed for Ni–Mo deposition on the samples in Fig. 1d, the electrodeposition process gave closely packed agglomerated particles, but did not completely cover the exposed silicon. Owing to the smaller exposed areas, for equal deposition times denser Ni–Mo particle films were formed on the top-exposed wires (Fig. 1e) than on fully exposed wires (Fig. 1d). As a limitation of our photocathode, it has to be noted that owing to the open, granular structure of the electrodeposited Ni–Mo (see Fig. 1e), the Si microwire arrays with spatioselectively deposited Ni–Mo are not stable in alkaline electrolyte solutions.

Photoelectrical (*J*–*V*) measurements

The microwire arrays with a radial n$^+$/p-junction were also fabricated as a solid-state Si PV cell, as described previously[6,8,9]. A schematic representation of the set-up is given in Supplementary Fig. 3. This allows the effects of the addition of Ni–Mo on the light-harvesting capabilities to

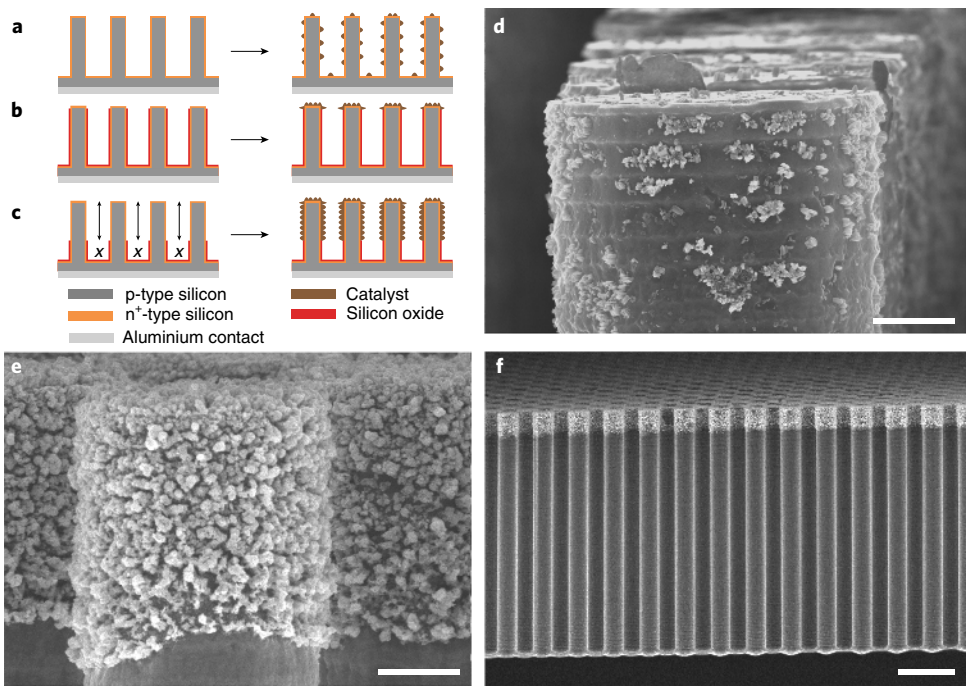

Fig. 1 | Electrodeposition of Earth-abundant catalysts, Ni–Mo, on Si microwire arrays with a radial junction. a–c, Fabrication process for completely exposed microwires (**a**), microwires passivated by SiO_2 with exposed tops (**b**), or samples with a defined exposed area in the range of 2–36 µm from the top (**c**). **d**, **e**, HR-SEM images of Si microwire arrays with n$^+$/p junctions with fully exposed microwires (sample A) after Ni-Mo electrodeposition of 30 s (**d**), and Ni–Mo solely on the tops of the microwire (sample B, 180 s deposition) (**e**). The scale bars in panels **d** and **e** are 1 µm. **f**, Zoom-out HR-SEM image of **e**; scale bar is 10 µm.

be assessed, without interference from other factors, such as electrolyte composition, bubble formation or contact resistances. We performed *J*–*V* measurements on both bare and catalyst-coated Si microwire arrays with fully (sample type A) or partially (sample type B) exposed wires (Fig. 2). Characteristic values of open-circuit potential (V_{oc}), short-circuit current (J_{sc}), FF and efficiency (η) are given in Supplementary Table 1.

For samples of fully exposed wires (A), the addition of Ni–Mo as a catalyst did not significantly influence the FF or V_{oc} of the *J*–*V* curve (see Fig. 2a and Supplementary Table 1). It solely blocked and/or scattered the light, as a consequence of which J_{sc} rapidly decreased for increasing Ni–Mo deposition time. When the deposition time was increased to 180 s, little light was converted into photocurrent, and the efficiency dropped to 1.1%. A deposition time of 180 s was used because it gave the highest catalyst activity (Supplementary Fig. 4) for *J*–*E* measurements in the dark.

For the Si microwire arrays in B samples, for which approximately the upper 1 μm of SiO_2 was spatioselectively removed and covered with Ni–Mo, the SiO_2 not only forms an electrical barrier that prevents catalyst deposition during the electrodeposition step, it also passivates the Si surface against charge carrier recombination and thereby enhances the PV efficiency[6,20–22]. *J*–*V* measurements performed after removal of the SiO_2 from the microwire tops only ('Bare' in Fig. 2b) showed an increase in V_{oc} as compared with non-passivated, fully exposed samples ('Bare' in Fig. 2a). Furthermore, the J_{sc} values were substantially higher, resulting in an increased efficiency of 13.0% (see Supplementary Table 1) for the Si microwire arrays with SiO_2.

As expected, high mass loading of electrodeposited Ni–Mo (180 s) affected only the J_{sc} (measurement set-up shown in Supplementary Fig. 3), owing to blocking of light absorption (see Fig. 2b). A Ni–Mo deposition time of 180 s yielded $J_{sc} = 28.3\ mA\ cm^{-2}$ for B samples as opposed to 4.2 $mA\ cm^{-2}$ for A samples under the same deposition conditions. A longer deposition time gave a higher catalyst loading on the microwires, yet the decrease in J_{sc} was substantially lower than for A samples.

Photoelectrochemical measurements

Photoelectrochemical (*J*–*E*) measurements under illumination were performed in 0.1 M aqueous H_2SO_4 for fully exposed Si microwire arrays with and without a complete coating of Ni–Mo catalyst (A samples) and for top-exposed samples with spatioselective catalyst deposition (B) (Fig. 3). The set-up is schematically represented in Supplementary Fig. 3, in which the lamp is always positioned perpendicular to the substrate, to have minimal reflection or refraction through the different materials.

All of the relevant values (V_{oc}, J_{ph}, FF, plateau current density and η_{IRC}) are tabulated in Supplementary Table 2. Ideally, a well-performing photocathode has the same characteristics (J_{ph} or J_{sc}, V_{oc} and FF) as the underlying PV cell. Therefore, ideal regenerative cells (IRCs) are fully analogous to the solid-state PV cells described and measured above, and the efficiency (η_{IRC}) of these systems is described by a similar equation as used to describe the efficiency of a PV device, (see equation (1))[4].

$$\eta_{IRC} = \frac{V_{oc} J_{ph}\left(E_{H_2/H^+}\right) FF}{P_{in}} \quad (1)$$

The values of FF, V_{oc} and $J_{ph}(E_{H2/H+})$ (that is, the current density at 0 V versus RHE) in equation (1) are referenced to the equilibrium potential of the half-reaction being performed at the photocathode, and P_{in} is the light power input (AM 1.5 G, 100 $mW\ cm^{-2}$).

Bare Si microwire arrays only produced H_2 at a large overpotential (see Fig. 3a,b) which exemplifies once more the need for an HER catalyst. For sample type A, the incorporation of the Ni–Mo catalyst with a deposition time as short as 10 s enhanced the H_2 production tremendously. This is witnessed by an increase in the photocurrent (J_{ph}) at 0 V versus RHE as compared with a bare sample. At a high overpotential, the performance of the underlying PV cell limits J_{ph} (that is, J_{ph} reaches a plateau), and the J_{ph} value matches well with the J_{sc} value of the same measured solid-state PV cell (see Supplementary Tables 1 and 2 for plateau current densities). The FF increases substantially for a photocathode sample when coated with Ni–Mo (~12% FF), although the values are lower than the values reached for the solid-state PV cell (~65% FF). Only when the deposition time is increased to180 s does the FF increase to 45%. Furthermore, the V_{oc} of A samples with deposition times up to 30 s is lower (~0.30 V versus RHE) than that of the PV cell (~0.45 V). The low V_{oc} is probably due to a pinch-off effect, which has been described previously for Ni particles (< 50 nm) on an n-type semiconductor [23]. Here we observed a similar particle size (<50 nm) on n-type Si by SEM (Supplementary Fig. 1). The V_{oc} shifts to 0.42 V versus RHE when the deposition time is increased (180 s). Interestingly, even though J_{ph} is the lowest (2.7 $mA\ cm^{-2}$) for the 180 s deposition time, η_{IRC} (1.0%) is the highest of all samples of type A, owing to the high FF value and increased V_{oc}.

Figure 3b presents the *J*–*E* measurements of the microwire arrays with and without the spatioselectively deposited catalysts Ni–Mo and Pt (B samples), recorded under illumination. Supplementary Table 2

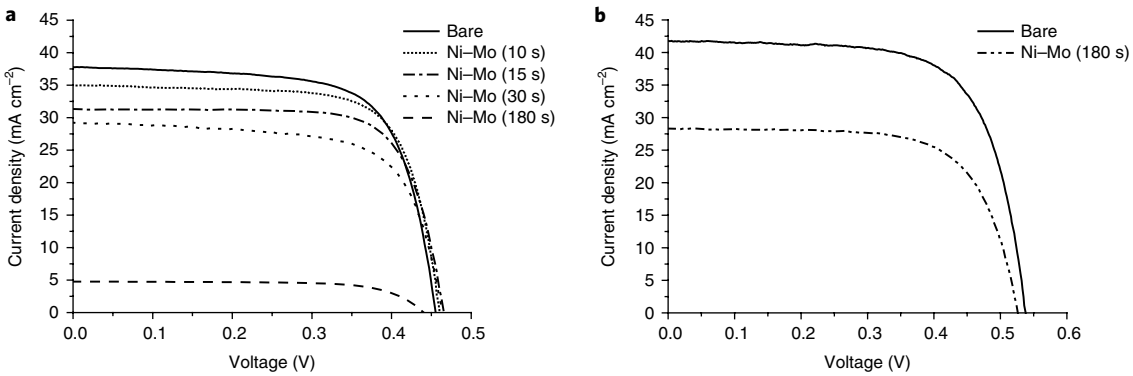

Fig. 2 | Photoelectrical *J*–*V* measurements of Si microwire arrays with radial n⁺/p-junctions. a, *J*–*V* measurement of photocathodes with and without electrodeposited Ni–Mo, using the deposition times shown, on fully exposed Si microwires; **b**, *J*–*V* measurement of photocathodes with and without Ni–Mo electrodeposited for 180 s spatioselectively on top-exposed arrays. Both panels show data measured using AM 1.5G illumination. Each line is the average of at least four different samples prepared with the same settings.

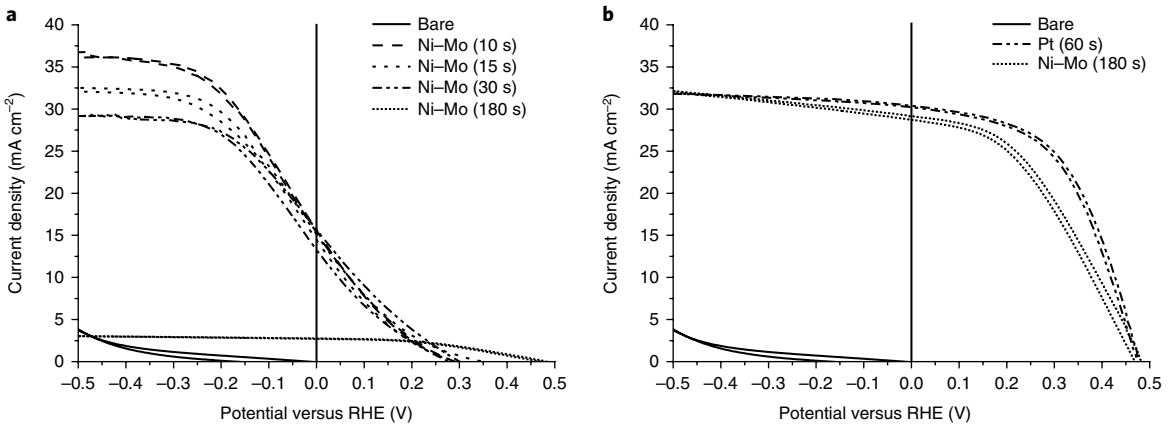

Fig. 3 | Current density J_{ph} versus potential for Si microwire array devices with radial n$^+$/p-junctions measured in cyclic potential sweeps. **a**, Measurements of photocathodes with and without electrodeposited Ni–Mo, using the deposition times shown, on fully exposed Si microwires; **b**, measurements of photocathodes with and without Pt or Ni–Mo electrodeposited, using the deposition times shown, spatioselectively on top-exposed arrays. Both panels show data measured using AM 1.5G illumination and collected in 0.1 M H_2SO_4, referenced to the RHE potential. The vertical line is a guide to the eye at 0 V versus RHE.

contains the compiled parameters of Fig. 3b. Again, the Si microwire array with spatioselectively etched SiO_2 without a catalyst exhibits a negligible J_{ph} at a potential of 0 V versus RHE. In contrast, deposition of either Ni-Mo or Pt at the top of the microwire arrays leads to a substantial increase of J_{ph} at 0 V versus RHE. Furthermore, the V_{oc} values for samples with locally deposited catalysts are substantially higher (~0.49 V versus RHE) than those observed for A samples with the catalyst deposited along the complete microwire length (~0.30 V versus RHE). This is attributed to replacement of most of the silicon-electrolyte interface by a passivation layer. The values for V_{oc}, FF and J_{ph} are in good agreement with the data for solid-state PV cells (see Supplementary Tables 1 and 2). A chopped light experiment, shown in Supplementary Fig. 5, together with a continuous measurement in the light and dark, shows that the latter two overlap nicely with the chopped light experiment, and that the dark leakage current is limited by a proper n$^+$/p junction. Furthermore, to demonstrate that we stay within the reductive limit, we added a graph with extended x and y axes, from which it is clear that the cyclic voltammetry (CV) scan returns to ~0 mA cm^{-2} for the Ni–Mo samples (see Supplementary Figure 6).

For comparison, Pt was also spatioselectively electrodeposited on the top-exposed microwires. Although it is a rare and precious metal in contrast to Ni and Mo, Pt is one of the best-performing HER catalysts, as is already observed in the dark J–E measurements (Supplementary Fig. 4). The η_{IRC} for B samples with a Pt catalyst is 7.1%. The use of spatioselectively deposited Ni–Mo as a catalyst enhances the photoelectrochemical output tremendously as compared with A samples. The increase is mainly reflected in the FF of the curve, which increases from 12% to 47%. The best-performing microwire array with Ni-Mo has a V_{oc} of 0.48 V, J_{sc} = 29.1 mA cm^{-2} and a fill factor of 47%, which results in η_{IRC} = 6.8%, which is highly comparable to the sample with Pt. The stability for 72 h and the Faradaic efficiency for HER of sample B have been tested as shown in Supplementary Figs 7 and 8.

To gain more mechanistic insight into the parameters affecting the efficiency of the HER half-cell based on spatioselective coverage of Si microwires, we investigated the influences of the microwire pitch, in the range of 8 to 24 µm, and the spatioselective Ni–Mo coverage over these microwires, in the range of 2 to 36 µm as measured from the top of the wires (see Fig. 1c). These variations were made using a special fabrication method (Fig. 1c)[24], because it turned out that the procedure in Fig. 1b, which uses a spin-coated polymer, had to be optimized separately for each geometry. The method is described in more detail in the Methods section. Two exemplary HR-SEM images are given in Fig. 4a,b, with 19 µm pitch and 18 µm Ni–Mo coverage, and with 24 µm pitch and 36 µm Ni–Mo coverage, respectively, which show the great control over the deposition technique.

The wire coverage with Ni–Mo was varied at different pitches, and the catalyst activity was measured in the dark by contacting the emitter (n$^+$-Si, schematic set-up given in Supplementary Fig. 3) as the working electrode. All graphs of current density versus potential for all combinations (six different pitches and five different coverages) can be found in Supplementary Fig. 9. To summarize the effect of microwire pitch and coverage on the catalyst activity, current densities of all combinations are plotted at one potential, 50 mV versus RHE; see Fig. 4c (red line in Supplementary Fig. 9). Clearly, to obtain optimal electrocatalytic activity, a trade-off has to be made between Ni–Mo coverage and microwire pitch. Smaller pitches are better, independent of covered wire length, but to overcome the limited activity of Ni–Mo at larger pitches (lower right corner of Fig. 4c), a higher coverage of the microwire is required (upper right corner of Fig. 4c).

The fully finished microwire photocathodes with spatioselectively deposited catalyst were also measured as PV cells, without the electrolyte (a schematic set-up is depicted in Supplementary Fig. 3). The J–V graphs of all combinations tested can be found in Supplementary Fig. 10. As with B samples, there was only a minor influence of the presence of Ni–Mo on FF and V_{oc}. To assess the impact of the microwire coverage and pitch on the photovoltaic performance of the samples, in Fig. 4d just the J_{sc} is shown in a contour plot, from which it becomes apparent that J_{sc} increases with increasing pitch and with decreasing degree of catalyst coverage (lower right corner of Fig. 4d). Conversely, the lower the microwire pitch and the higher the coverage, the lower is the current density (upper left corner of Fig. 4d).

The contour plot Fig. 4e of overall device efficiency η_{IRC} versus pitch and wire coverage shows three domains (the J–E graphs of all combinations are found in Supplementary Fig. 11). In the lower right corner of Fig. 4e, the overall efficiency is dominated by the FF, which is a direct consequence of the limited amount of active catalyst (see also Fig. 4c). In detail, a photocathode behaves as the superposition of the catalyst behaviour in the dark (Supplementary Fig. 9) and the underlying PV cell (Supplementary Fig. 10). Because the resistances of the PV cells are found to be lower than the resistance imposed by the catalyst, we conclude that the FF of a

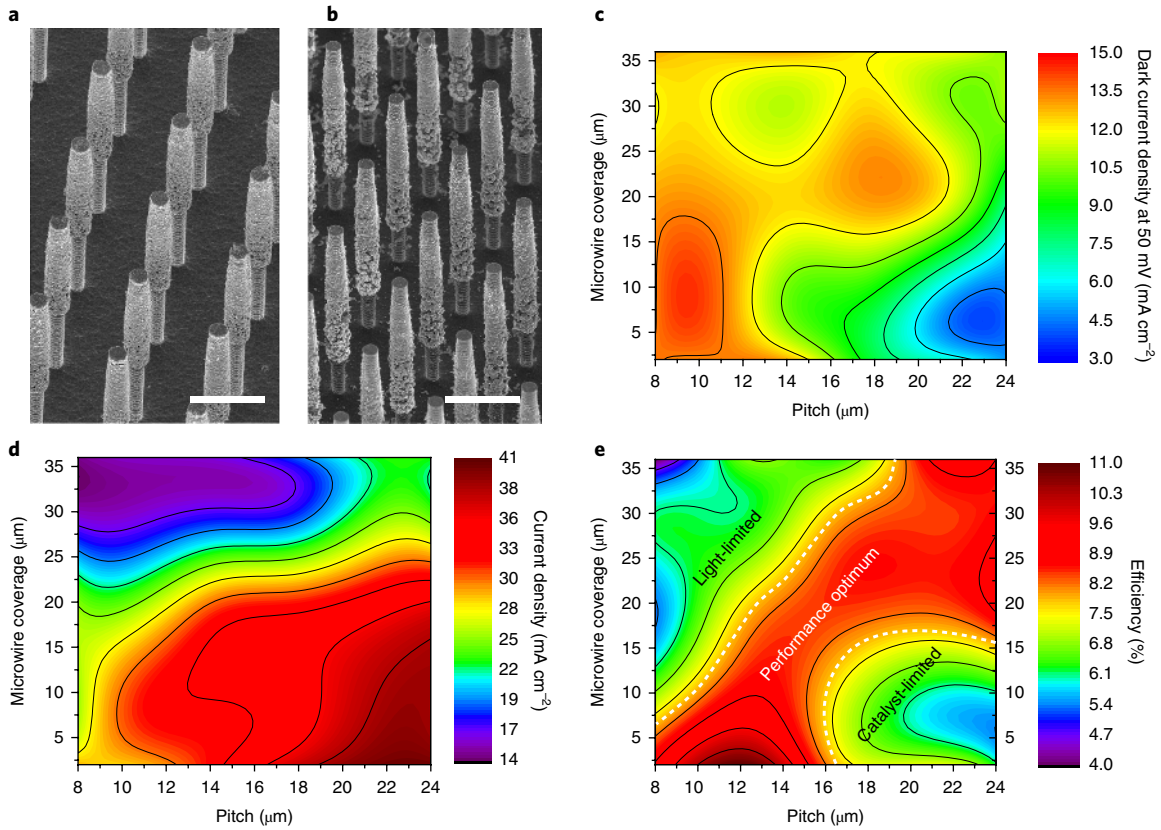

Fig. 4 | Deconvolution of catalytic activity and light-absorption losses in a Si microwire photocathode. HR-SEM images of electrodeposition of Earth-abundant catalyst (Ni–Mo) on Si microwire arrays with a radial junction. The microwires were passivated by SiO_2 on the bottom part, while Ni–Mo was electrodeposited at the top. **a**, Centre-to-centre distance between the microwires is 19 μm, and the top 18 μm of the microwires is covered with catalyst. **b**, Centre-to-centre distance between the microwires is 24 μm, and the top 36 μm of the microwires is covered with catalyst. Scalebars in **a** and **b**: 15 μm. **c**, Contour plot of current density at 50 mV versus RHE as a function of pitch and wire coverage. **d**, Contour plot of the current density J_{sc} as a function of pitch and wire coverage. **e**, Contour plot of the overall device HER efficiency, η_{IRC}, as function of pitch and wire coverage for all tested combinations. All contour plots are interpolated (cubic spline) from measurements on different devices.

photocathode is mainly determined by the resistance that the catalyst imposes on the underlying PV cell. There is an analytical approximation to calculate the FF when the values of series resistance (R_s), V_{oc} and short-circuit current (I_{sc}) are known[25]. The resistance R_s was here obtained for each variation by linearizing every data series in Supplementary Fig. 9 in the range between 0 and 50 mV. The calculated (FF_s) and measured (FF) fill-factor values are tabulated in Supplementary Table 3. In all cases, the calculated values correspond well to the measured ones, thus supporting the idea that limitation by the catalyst is the main contributor to the fill factor. In the upper left corner of Fig. 4e, the overall efficiency is limited by light absorption. This is a direct consequence of reduced light absorption of the microwire array, because the catalyst blocks the incoming light, as is clear from Fig. 4d. Between these two zones, a region of optimal performance is found in which both the catalysis and the light absorption perform close to their maximum. In this zone, a pitch of 12 μm and a spatioselective coverage of 2 μm on the upper part of the 40-μm-long Si microwires results in the highest ideal regenerative cell efficiency (10.8%).

To highlight the importance of catalysts on silicon microwires and nanowires in hydrogen-producing half-cells, we present an overview of reported data, subdivided into three categories: with Ni–Mo; with Pt; or with any other catalyst. The three best-performing systems of each category are given in Table 1. To the best of our knowledge, our system outperforms previous half-cells constructed from either Si microwires or nanowires. A more complete list is given in Supplementary Table 4.

Table 1 | Compilation of microwire-based and nanowire-based hydrogen-producing half-cells

Configuration	V_{oc} (mV)	J_{ph} (mA cm^{-2})	FF (%)	η_{IRC} (%)	Reference
Ni–Mo					
n^+/p-Si MWs	495	35.5	62	10.8	This paper
n^+/p-Si MWs	420	14.3	48	2.9	Ref. [2]
n^+/p-Si MWs	485	10.3	45	2.2	Ref. [12]
Pt					
n^+/p-Si MWs	480	30.4	51	7.1	This paper
n^+/p-Si MWs	540	15.0	71	5.8	Ref. [30]
n^+/p-Si MWs	510	20.2	49	5.0	Ref. [2]
Other					
p-Si NWs/$N_{12}P_5$	400	21.0	36	3.0	Ref. [31]
p-Si NWs/CoP	407	15.6	27	2.9	Ref. [32]
p-Si NWs/FeP	470	13.9	45	2.8	Ref. [33]

Measurements done under AM 1.5G simulated sunlight in their best-performing electrolyte. MW, microwire; NW, nanowire.

The efficiencies, if not given in the original literature reference, were calculated from the respective reported data, according to equation (1).

Furthermore, as a proof of concept to show the feasibility of implementation of our developed photocathodes in a fully functioning solar-to-fuel device, we fabricated a backside-illuminated photoanode, a frontside-illuminated photocathode, separated by a membrane (Supplementary Fig. 12). We fabricated a bismuth vanadate ($BiVO_4$) photoanode according to a previously reported procedure[26], to overcome the mismatch between the preferred pH values for the photoanode (high pH) and photocathode (low pH), a bipolar membrane has been used between the compartments, as described in a previous study[27]. For this basic, wired solar-to-fuel device, we observed a stable, unbiased water-splitting efficiency of 2.1% over the course of an hour. For further details, see the Supplementary Discussion.

Discussion

We have designed, fabricated and experimentally validated a photoelectrode architecture that circumvents the trade-off between electrocatalytic activity of an opaque catalyst and optical absorption, parameters that determine FF and J_{ph}, respectively. By spatially and functionally decoupling light absorption and catalytic activity on high-aspect-ratio silicon microwires with a radial n^+/p-junction, efficient solar-driven hydrogen evolution has been achieved. This was first demonstrated and compared with an architecture which consisted of a high mass loading of Ni–Mo or Pt deposited spatioselectively on the upper 2 µm of microwire arrays. This concept clearly demonstrates that precious metals (such as Pt) are not necessary to construct an efficient H_2 photocathode.

Two factors have been identified as limiting for the performance of photocathodes with opaque catalysts, insufficient catalyst loading (FF) and parasitic light absorption (J_{ph}) by the catalyst. The first was found to dominate when the microwire arrays had a large pitch and only small parts of the wires were covered by catalyst. At a low pitch and high catalyst coverage, the performance was clearly limited by the light absorption performance of the underlying Si microwire photon absorber.

The photocathode configuration presented here has been functionally assessed upon frontside illumination in an acidic electrolyte. The relevance of the spatioselective catalyst deposition method thus depends on an overall device configuration in which frontside illumination is used. Therefore, we implemented our photocathode design in a full device using a wired device geometry. We have successfully demonstrated here such a full solar-to-fuel device architecture, and stable, unbiased water splitting has been shown over the course of an hour.

Our future research will focus on increasing the stability of the Si microwire photocathode in alkaline electrolytes and on increasing the produced photovoltage. The latter can be achieved, for example, by using a microwired tandem cell constructed of amorphous Si on top of crystalline Si microwires[28]. The silicon materials used in that study should be compatible with the fabrication process presented in the current study, possibly with adaptation of the patterning process parameters and/or the masking materials. Parasitic light absorption within the catalyst material should be prevented by spatioselective catalyst deposition, while maintaining high catalytic activity, as is demonstrated in the current study.

We have demonstrated that, by careful design at the microscale, the chosen architecture provides high performance for an HER half-cell made entirely of Earth-abundant materials. The concept should also be applicable to other material combinations, provided that fabrication methods can be found for those materials to achieve structuring at the right scale. The best-performing HER half-cell investigated here consisted of a Ni–Mo catalyst on the upper 2 µm and a pitch of 12 µm, and demonstrated a η_{IRC} of 10.8%.

Methods

Fabrication of radial n+/p junctions in Si microwire arrays. Supplementary Fig. 13 gives a schematic representation of the fabrication and passivation of an array of microwires with radial n^+/p junctions. Substrates made of p-type Si{100}, with a resistivity of 5–10 Ω cm, 100 mm diameter, 525 µm thickness, single side polished (Okmetic Finland), were prepared as previously reported[8,9]. In short, substrates were cleaned according to a standard procedure, and covered with 100 nm silicon-rich silicon nitride (SiN_x) by low-pressure chemical vapour deposition (LPCVD; 150 mTorr, flow 77.5 standard cubic centimetre per minute (sccm) of SiH_2Cl_2, 20 sccm of NH_3 and 150 sccm of N_2 at 850 °C, 25 min). The SiN_x on the front side of the wafer was removed by reactive ion etching (RIE, Adixen AMS100DE; substrate temperature 10 °C, 20 sccm C_4F_8, 15 sccm CH_4, 150 sccm He, pressure 8.5×10^{-3} mbar, inductively coupled plasma (ICP) power 2,800 W and capacitively coupled plasma (CCP) power 350 W for 60 s), and the substrate was cleaned by oxygen plasma (30 min; Tepla360 barrel etcher). By means of standard photolithography, squares (5×5 mm^2) with hexagonally packed circles (4 µm diameter, and varying pitch from sample to sample between 6 and 24 µm) were defined in a photoresist polymer (Olin 906-12). Silicon microwires (40 µm in height) were etched into the silicon substrate by deep reactive ion etching (DRIE, Bosch process; a cyclic process using SF_6 for silicon etching and C_4F_8 to create a passivation layer on the sidewalls) and the substrates were cleaned subsequently in oxygen plasma (30 min). The n^+/p junctions were formed by the deposition of phosphorus oxide (LPCVD). A mixture of 330 sccm PH_3 and 50 sccm O_2 was supplied for 45 min at 350 mTorr in order to deposit a phosphorus oxide glass on the silicon surface. The substrate was annealed at 1,050 °C for 15 min to accomplish diffusion of the dopant into the silicon microwire array to form the appropriate radial junction. Before the deposition of the passivation layer, the dopant oxide was stripped in BHF solution (10 min), upon which the wafers returned to their hydrophobic state (Supplementary Fig. 13). Subsequently, the wafers were cleaned by immersion in fuming 99% nitric acid (HNO_3, 2×5 min), boiling 69% nitric acid (10 min) and immersion in 1% aqueous hydrofluoric acid (HF) to remove the native oxide (1 min). The 100 nm passivation layer of SiO_2 was applied by LPCVD and is described in more detail below. After selective removal of the surface passivation coating from the tops of the microwires, a Ni–Mo alloy was deposited on the microwires by electrodeposition; for more details, see below. Finally, ohmic contacts (1 µm; Al/Si, 99/1%) were sputtered (Oxford PL400) on the front and back sides of the wafer.

LPCVD of SiO_2 passivation layer. Conformal deposition of a silicon oxide (SiO_2) film was done by means of LPCVD. SiO_2 was deposited at 725 °C with a 50 sccm tetraethyl orthosilicate flow (200 mTorr, 8.1 nm min^{-1} deposition rate). The total thickness of SiO_2 was set to 100 nm.

Local removal of SiO_2 from the tops of Si microwire arrays. To selectively remove SiO_2 from the tops of the microwires, the following protocol was applied. HMDS (hexamethyldisilazane) was spin-coated between the wires (4,000 rpm, 2 min), and subsequently AZ9260 photoresist was spin-coated (1,000 rpm, 4 min). The samples were dried overnight at 10^{-3} mbar at room temperature. Tthe photoresist was then removed around the microwire arrays by masking the arrays with squares of 5×5 mm^2. The samples were exposed to light (3×10 s ultraviolet exposure, 10 s delay between exposure cycles) and developed (7 min). The remaining photoresist within the microwire arrays was exposed to light with a blank mask (3×10 s ultraviolet exposure, 10 s delay between exposure cycles). The resist layer between the microwires was reduced in thickness using RIE for ~3 min (100 sccm O_2, 100 mTorr, 25 W, 10 °C), until the desired height of photoresist around the microwires was obtained (Supplementary Fig. 13; see Supplementary Fig. 14 for HR-SEM images). SiO_2 was selectively removed from the exposed tops by wet etching in BHF (~1 min, etch rate 210 nm min^{-1}). The remaining photoresist layer was stripped by 10 min ultrasonication in acetone, followed by 10 min ultrasonication in isopropanol and spin-drying. The selectively etched microwire arrays showed clearly exposed tops (Supplementary Fig. 14).

Removal of SiO_2 over a defined length of Si microwire arrays. Supplementary Fig. 15 gives a schematic representation of the fabrication and passivation of an array of microwires with radial n^+/p junctions and spatioselective catalyst deposition. To selectively electrodeposit a catalyst on microwires, a SiO_2 layer is used as masking layer for the electrodeposition of the catalyst. First, microwires are coated with three layers deposited by LPCVD, where each layer will form a hard mask for patterning the underlying layer. First, 100 nm of SiO_2 is deposited (400 mTorr, 40 sccm of tetraethoxysilane (TEOS) and 30 sccm of N_2 at 725 °C, 10 min), followed by 60 nm of silicon-rich silicon nitride (SiRN; 150 mTorr, 77.5 sccm of SiH_2Cl_2, 20 sccm of NH_3 and 150 sccm of N_2 at 850 °C, 12 min), followed by 180 nm of polycrystalline silicon (250 mTorr, 50 sccm of SiH_4 and 250 sccm of N_2 at 590 °C, 55 min). Lastly, 134 nm of SiO_2 is formed by wet thermal oxidation (900 °C, 45 min) which consumes part of the polysilicon layer (see Supplementary Fig. 15).

The first outer layer of SiO_2 is selectively removed from the top of the wires by ion beam etching under an angle (Oxford Ionfab 300Plus system, 2×10^{-4} Torr; neutralizer: 5 sccm argon, 100 mA; RF plasma: 125 W; beam: 5 sccm argon, 50 mA, acceleration 300 V, angle of the beam with respect to surface normal 70°, substrate rotating at 5 rpm; etching time: 10 min) and the rate of silicon removal was

monitored using secondary ion mass spectrometry. Subsequently, the sample was etched for 5 min in 1% aqueous HF solution (see Supplementary Fig. 15).

Retraction of polysilicon (approximately 500 nm min^{-1}) was done in 25% aqueous tetramethylammonium hydroxide (TMAH) solution at 70 °C, varied between 4 and 72 min depending on the required height of the catalyst (see Supplementary Fig. 15, where *X* denotes the retraction height as measured from the top of the microwire). Next, the outer SiO_2 is removed by etching for 150 s in BHF (12.5 wt% HF in NH_4F), followed by SiRN etching, 25 min at 180 °C in 85% aqueous H_3PO_4 solution. The polysilicon is removed by etching for 1 min in the TMAH solution as described above, and the pattern is transferred to the inner SiO_2 layer by etching for 2 min in BHF. Finally, the SiRN is removed by etching 25 min in a hot concentrated H_3PO_4 solution. After each wet etching step, the wafers were thoroughly rinsed in deionized water, and then directly transferred to the next wet etching bath.

Electrical contacts. To ensure ohmic contact to the solar cells, 1 µm aluminium/silicon alloy (99% Al, 1% Si) was sputtered (Oxford PL 400) on the front and back sides of each specimen, where on the front side a shadow mask was applied to protect the wire arrays from coating. In this way, a square electrode was formed around the wire array. Directly before coating, all native silicon oxide was stripped from the silicon surface by etching for 1 min in 1 wt% aqueous HF solution.

Catalyst deposition. Ni–Mo was deposited by electrodeposition directly after forming the ohmic contacts as described above, to limit formation of a new oxide layer on the silicon as much as possible. The Ni–Mo catalyst was deposited in a two-electrode set-up, by solely contacting the n^+-Si emitter through the aluminium contact on the front. The counter-electrode was a Pt mesh. The electrodeposition bath consisted of an aqueous solution of 1.3 M nickel(II) sulphate hexahydrate, 0.5 M boric acid, and 25 mM sodium molybdate in Milli-Q water. The samples were covered with a ring so that only a circular area of 6 mm diameter was exposed to the electrolyte. Electrodeposition of Ni–Mo catalyst on the Si microwires was performed at a constant current of 5.5 mA (20 mA cm^{-2} with respect to projected sample area not covered by the ring) for time periods described in Supplementary Table 5.

Platinum was deposited from an aqueous solution of 5 mM hexachloroplatinic acid (H_2PtCl_6) and 0.5 M sodium sulfate (Na_2SO_4), potentiostatically at −0.7 V. Charge densities of 130 mC cm^{-2} were supplied.

***J–V* measurements.** To measure the electrical characteristics of the coated Si microwires, samples were positioned perpendicular to a light source (see Supplementary Fig. 3). *J–V* measurements were recorded on a VersaSTAT 4 potentiostat using a linear voltage sweep from −0.7 to 0.7 V at a rate of 0.2 V s^{-1}. The light intensity was calibrated to AM 1.5G illumination at the position of the sample, using the calibrated light source described below.

***J–E* measurements.** The coated microwire photocathodes were photoelectrochemically tested using a potentiostat (VersaSTAT 4) in a three-electrode configuration, in which the microwire photocathode with an exposed projected surface area of 0.28 cm^2 acted as the working electrode (WE), a platinum wire mesh as the counter-electrode (CE) and an Ag/AgCl electrode as the reference electrode (RE). The electrolyte used was 0.1 M aqueous sulfuric acid (H_2SO_4), pH 1. A set-up as shown in Supplementary Figure 3 was used for dark *J–E* measurement;, the n^+-Si emitter was contacted as the WE, directly through the aluminium contact on the front. For each sample, five full cyclic voltammetry measurements were done at a scan rate of 10 mV s^{-1}.

For *J–E* measurements under illumination, the backside p-Si base was contacted through the aluminium contact on the back. Five full cyclic voltammetry measurements were done at a scan rate of 10 mV s^{-1}. Samples were positioned perpendicular to a solar spectrum light source as described below. The configuration is shown in Supplementary Fig. 3. The light intensity was calibrated to AM 1.5G illumination at the position of the sample. Here, continuous scans were recorded instead of chopped light. To show the similarity, one scan is taken under chopped light and overlaid with a dark and light *J–E* measurement in Supplementary Fig. 5.

The water layer on top of the sample was 15 mm thick. The absolute light absorption by the solution would lead to a decrease of 3 mA cm^{-2} if it is assumed that every photon leads to an electron. The absorption was calculated from the Lambert–Beer relation and integrated over the solar spectrum in the range of 300–1,200 nm (see Supplementary Fig. 16)[29].

Light source and calibration. The light source that was used is a 300W xenon arc light source, fitted with Air Mass filter (AM 1.5G) from Newport, Oriel Instruments. Upon installation, the lamp was calibrated by Newport. Before every measurement, the lamp was checked by a calibrated reference solar cell (91150V). The 91150 V reference cell and meter consist of a readout device, a 2×2 cm calibrated solar cell made of monocrystalline silicon and a KG5 window. The cell is equipped with a thermocouple assembled in accordance with IEC 60904-2. The certification is accredited by the National Institute of Standards and Technology (NIST) to the ISO-17025 standard. It reads solar simulator irradiance in Sun units, whereby one Sun is equal to 1,000 W m^{-2} at 25 °C and AM 1.5 Global Reference.

The solar simulator was checked for spectral mismatch by a spectrometer (AvaSpec-ULS2048XL-EVO) fitted with a CC-VIS/NIR, slit size 10 µm, 1.4 nm resolution in the range 300–1,050 nm, an integration time of 8 ms and averaged over 60 scans. The spectral scan and an ASTM reference pattern are given in Supplementary Fig. 17. The current density (assuming 100% incident photon-to-current efficiency, IPCE) of the calibrated lamp and the ASTM spectrum match very well, 40.1 mA/cm^2 and 40.8 mA/cm^2 respectively, in the range of 300–1050 nm.

Gas chromatography. The reactor was connected to a gas chromatograph (Compact GC, Interscience), equipped with a Parabond Q column (10 m) and a thermal conductivity detector to determine the amount of H_2 in the argon carrier gas. 5 mL/min argon was flowed through the electrolyte and sampled every 90 s for the presence of H_2.

$BiVO_4$ and solar-to-fuel device. The photoanode was fabricated according to the procedure of ref. [26]. Precursor solutions were prepared by dissolving 0.2 M $Bi(NO_3)\cdot 5\,H_2O$ in acetic acid, and 28.5 mM $VO(acac)_2$ and 1.5 mM $MoO_2(acac)_2$ (acac = acetylacetonate) in acetyl acetone. Aliquots of these precursor solutions were mixed to yield Bi:(V + Mo) = 1:1 (atomic ratio). For fabrication of a 5% Mo-doped $BiVO_4$ film, 80 µl of this mixture was dropped on a fluorine-doped tin oxide (FTO) glass (2×2 cm^2) and dried under a stream of N_2 for 15 min. The FTO glass was cleaned by using KOH (0.1 M) and EtOH in a ratio of 1:5, washed with copious amounts of deionized water, and blow-dried. The greenish transparent precursor film was calcined at 550 °C for 25 min to form a yellow $BiVO_4$ film. A NiOOH/FeOOH co-catalyst was deposited by photo-assisted electrodeposition under AM 1.5G illumination. FeOOH was deposited from a 0.1 M $Fe(SO_4)_2\cdot 7H_2O$ solution for 15 min at 0.25 V versus Ag/AgCl. Subsequent deposition was made with NiOOH from a 0.1 M $Ni(SO_4)_2\cdot 6H_2O$ solution at 0.11 V versus Ag/AgCl.

The Si microwire photocathode was fabricated as described above, with a microwire pitch of 12 µm and only the upper 2 µm covered with Ni–Mo. A commercial bipolar membrane was used (Fumasep FBM, FumaTech), which was conditioned in 1.0 M K_2SO_4 solution prior to installing in the water-splitting cell.

Data availability. The data that support the plots within this paper and other findings of this study are available from the corresponding author upon reasonable request.

Received: 18 February 2017; Accepted: 28 November 2017;
Published online: 15 January 2018

References

1. Walter, M. G. et al. Solar water splitting cells. *Chem. Rev.* **110**, 6446–6473 (2010).
2. Shaner, M. R., McKone, J. R., Gray, H. B. & Lewis, N. S. Functional integration of Ni–Mo electrocatalysts with Si microwire array photocathodes to simultaneously achieve high fill factors and light-limited photocurrent densities for solar-driven hydrogen evolution. *Energy Environ. Sci.* **8**, 2977–2984 (2015).
3. Roske, C. W. et al. Comparison of the performance of CoP-coated and Pt-coated radial junction n^+p-silicon microwire-array photocathodes for the sunlight-driven reduction of water to H_2(g). *J. Phys. Chem. Lett.* **6**, 1679–1683 (2015).
4. Coridan, R. H. et al. Methods for comparing the performance of energy-conversion systems for use in solar fuels and solar electricity generation. *Energy Environ. Sci.* **8**, 2886–2901 (2015).
5. Battaglia, C., Cuevas, A. & De Wolf, S. High-efficiency crystalline silicon solar cells: status and perspectives. *Energy Environ. Sci.* **9**, 1552–1576 (2016).
6. Vijselaar, W., Elbersen, R., Tiggelaar, R. M., Gardeniers, H. & Huskens, J. Photo-electrical characterization of silicon micropillar arrays with radial p/n junctions containing passivation and anti-reflection coatings. *Adv. Energy Mater.* **7**, 1601497 (2016).
7. Chen, Y. K., Sun, K., Audesirk, H., Xiang, C. X. & Lewis, N. S. A quantitative analysis of the efficiency of solar-driven water-splitting device designs based on tandem photoabsorbers patterned with islands of metallic electrocatalysts. *Energy Environ. Sci.* **8**, 1736–1747 (2015).
8. Elbersen, R. et al. Controlled doping methods for radial p/n junctions in silicon. *Adv. Energy Mater.* **5**, 1401745–1401753 (2015).
9. Elbersen, R., Vijselaar, W., Tiggelaar, R. M., Gardeniers, H. & Huskens, J. Effects of pillar height and junction depth on the performance of radially doped silicon pillar arrays for solar energy applications. *Adv. Energy Mater.* **6**, 1501728 (2016).
10. *Nickel Plating Handbook* Vol. 1, 80 (Nickel Institute, Toronto, Canada, 2014).
11. McKone, J. R. et al. Evaluation of Pt, Ni, and Ni–Mo electrocatalysts for hydrogen evolution on crystalline Si electrodes. *Energy Environ. Sci.* **4**, 3573–3583 (2011).
12. Warren, E. L., McKone, J. R., Atwater, H. A., Gray, H. B. & Lewis, N. S. Hydrogen-evolution characteristics of Ni-Mo-coated, radial junction, n+p-silicon microwire array photocathodes. *Energy Environ. Sci.* **5**, 9653–9661 (2012).

13. Hoare, J. P. Boric-acid as a catalyst in nickel plating solutions. *J. Electrochem. Soc.* **134**, 3102–3103 (1987).
14. Fan, C., Piron, D. L., Sleb, A. & Paradis, P. Study of electrodeposited nickel–molybdenum, nickel–tungsten, cobalt–molybdenum, and cobalt–tungsten as hydrogen electrodes in alkaline water electrolysis. *J. Electrochem. Soc.* **141**, 382–387 (1994).
15. Podlaha, E. J. & Landolt, D. Induced codeposition. I. An experimental investigation of Ni–Mo alloys. *J. Electrochem. Soc.* **143**, 885––892 (1996).
16. Podlaha, E. J. & Landolt, D. Induced codeposition. II. A mathematical model describing the electrodeposition of Ni–Mo alloys. *J. Electrochem. Soc.* **143**, 893–899 (1996).
17. Podlaha, E. J. & Landolt, D. Induced codeposition. III. Molybdenum alloys with nickel, cobalt, and iron. *J. Electrochem. Soc.* **144**, 1672–1680 (1997).
18. Chen, Y., Shen, J. & Chen, N. X. The effect of Mo atoms in ternary nitrides with eta-type structure. *Solid State Commun.* **149**, 121–125 (2009).
19. Mishima, Y., Ochiai, S. & Suzuki, T. Lattice parameters of Ni(γ), $Ni_3Al(\gamma')$, and $Ni_3Ga(\gamma')$ solid solutions with the additions of transition and B-subgroup elements. *Acta Metallurgica* **33**, 1161–1196 (1985).
20. Schultz, O., Mette, A., Hermle, M. & Glunz, S. W. Thermal oxidation for crystalline silicon solar cells exceeding 19% efficiency applying industrially feasible process technology. *Prog. Photovoltaics* **16**, 317–324 (2008).
21. Benick, J., Zimmermann, K., Spiegelman, J., Hermle, M. & Glunz, S. W. Rear side passivation of PERC-type solar cells by wet oxides grown from purified steam. *Prog. Photovoltaics* **19**, 361–365 (2011).
22. Mack, S. et al. Properties of purified direct steam grown silicon thermal oxides. *Sol. Energy Mater. Sol. Cells* **95**, 2570–2575 (2011).
23. Garcia-Esparza, A. T. & Takanabe, K. A simplified theoretical guideline for overall water splitting using photocatalyst particles. *J. Mat. Chem. A* **4**, 2894–2908 (2016).
24. Westerik, P. J. et al. Sidewall patterning — a new wafer-scale method for accurate patterning of vertical silicon structures. *J. Micromech. Microeng.* **28**, 015008 (2017).
25. Green, M. A. Accuracy of analytical expressions for solar cell fill factors. *Solar Cells* **7**, 337–340 (1982).
26. Kim, J. H. et al. Hetero-type dual photoanodes for unbiased solar water splitting with extended light harvesting. *Nat. Commun.* **7**, 13380 (2016).
27. Vermaas, D. A., Sassenburg, M. & Smith, W. A. Photo-assisted water splitting with bipolar membrane induced pH gradients for practical solar fuel devices. *J. Mat. Chem. A* **3**, 19556–19562 (2015).
28. Veldhuizen, L. W., Vijselaar, W. J. C., Gatz, H. A., Huskens, J. & Schropp, R. E. I. Textured and micropillar silicon heterojunction solar cells with hot-wire deposited passivation layers. *Thin Solid. Films* **635**, 66–72 (2017).
29. Hale, G. M. & Querry, M. R. Optical constants of water in the 200-nm to 200-μm wavelength region. *Appl. Opt.* **12**, 555–563 (1973).
30. Boettcher, S. W. et al. Photoelectrochemical hydrogen evolution using Si microwire arrays. *J. Am. Chem. Soc.* **133**, 1216–1219 (2011).
31. Huang, Z. et al. $Ni_{12}P_5$ nanoparticles as an efficient catalyst for hydrogen generation via electrolysis and photoelectrolysis. *ACS Nano* **8**, 8121–8129 (2014).
32. Bao, X. Q., Fatima Cerqueira, M., Alpuim, P. & Liu, L. Silicon nanowire arrays coupled with cobalt phosphide spheres as low-cost photocathodes for efficient solar hydrogen evolution. *Chem. Commun.* **51**, 10742–10745 (2015).
33. Lv, C. et al. Silicon nanowires loaded with iron phosphide for effective solar-driven hydrogen production. *J. Mat. Chem. A* **3**, 17669–17675 (2015).

Acknowledgements

The Netherlands Organization for Scientific Research (NWO) is acknowledged for financial support (FOM projects 13CO12-1 and 13CO12-2, and MESA+ School for Nanotechnology grant 022.003.001). A. Milbrat and G. Mul are acknowledged for assistance with the gas chromatography measurements.

Author contributions

W.V., P.W., J.V. and E.B. performed the experimental work, W.V., P.W., N.R.T. and R.M.T. planned the project and performed the data analysis, W.V., H.G. and J.H. conceived the idea, and all authors contributed to the writing of the manuscript.

Competing interests

The authors declare no competing financial interests.

Additional information

Supplementary information is available for this paper at https://doi.org/10.1038/s41560-017-0068-x.

Reprints and permissions information is available at www.nature.com/reprints.

Correspondence and requests for materials should be addressed to H.G. or J.H.

Publisher's note: Springer Nature remains neutral with regard to jurisdictional claims in published maps and institutional affiliations.